Investigation on long-term extreme response of an integrated offshore renewable energy device with a modified environmental contour method

Liang Li[a], Zhi-Ming Yuan[a*], Yan Gao[a], Xinshu Zhang[b], Tahsin Tezdogan[a]

[a]*Department of Naval Architecture, Ocean and Marine Engineering, University of Strathclyde, UK*

[b]*School of Naval Architecture, Ocean and Civil Engineering, Shanghai Jiao Tong University, China*

Abstract

Considering the massive simulations required by the full long-term analysis, the environmental contour method is commonly used to predict the long-term extreme responses of an offshore renewable system during life time. Nevertheless, the standard environmental contour method is not applicable to the wind energy device due to the non-monotonic aerodynamic behaviour of the wind turbine. This study presents the development of a modified environmental counter method and its application to the extreme responses of a hybrid offshore renewable system. The modified method considers the variability of the responses by checking multiple contour surfaces so that the non-monotonic aerodynamic behaviour of the wind turbine is considered. The hybrid system integrates a floating wind turbine, a wave energy converter and two tidal turbines. Simulation results prove that the modified method has a better accuracy.

Keywords: extreme response, environmental contour method, renewable energy, floating wind turbine, wave energy converter, tidal turbine

1. Introduction

Powered by the increasing global pursuit of offshore renewable energy, various types of ocean energy systems are developed, including the floating wind turbine, the wave energy converter and the tidal turbine. Studies on an individual energy system have been fully conduced [1-5]. Nevertheless, producing power from a single type of ocean energy resource faces the problem of high cost and low harvesting efficiency. Therefore, the concept of integrated offshore renewable energy devices is proposed.

Nehrir et al. [6] presented a review of hybrid renewable energy systems, in term of configurations, control and applications. Aubault et al. [7] incorporated an oscillating-water-column WEC into a semi-submersible floating wind turbine. They showed that the overall cost could be reduced by sharing the mooring system and the power infrastructure. Muliawan et al. [8] studied the dynamic response and the power performance of the so-called STC concept in various operational conditions. Their simulation results revealed a synergy between wind and wave energy generation. Experimental and numerical

* Corresponding author at: Dep. of Naval Architecture, Ocean & Marine Engineering, University of Strathclyde.
Henry Dyer Building, G4 0LZ, Glasgow, UK.
Tel: + 44 (0)141 548 3308
E-mail address: zhiming.yuan@strath.ac.uk

studies of the STC in survival mode were conducted by Wan et al. [9, 10]. Wan et al. [11] investigated the hydrodynamic responses of STC under operational conditions. Michailides et al. [12] incorporated a flap-type WEC to a semi-submersible floating wind turbine and investigated the effect of WECs on the response of the integrated system. Their study showed that the combined operation of the rotating flaps resulted in an increase of the produced power without affecting the critical response quantities of the semi-submersible platform significantly. Li et al. [13] proposed a hybrid offshore renewable energy device by combining a floating wind turbine, a WEC and two tidal turbines. It was shown that the overall power production was increased while the platform motions were reduced. The short-term extreme response of this concept was further examined by Li et al. [14]. Bachynski and Moan [15] studied the effects of three point-absorber WECs on a TLP floating wind turbine in operational and 50-year extreme environmental conditions, in terms of power production, structural loads and platform motions.

For the design of offshore renewable energy devices, a long-term analysis is necessary to estimate the life-time fatigue damage and the extreme structural responses. The long-term analysis integrates the short-term response with a given environmental distribution model to value the life-time values, which is the basic idea of the so-called full long-term analysis (FLTA). Coe et al. [16] performed a full long-term analysis on the dynamic responses of a WEC. Agarwal and Manuel [17] investigated the extreme response of an offshore floating wind turbine with the FLTA. Nevertheless, the FLTA requires massive simulations of short-term response to cover every combination of environmental parameters. It is inefficient and many alternative methods have been developed. Videiro and Moan [18] proposed a simplified FLTA method which assumed that only the environmental conditions around a critical condition have influence on the extreme responses. Winterstein et al. [19] introduced an inverse first-order reliability method (IFORM). In their method, the uncertainties in the gross environment condition and the extreme response given the environment condition were decoupled. The IFORM is based on the transformation between a standardized normal space and a physical space (in which the variables are response and environmental parameters). All the possible combinations of variables at given a return period are firstly identified in the normal space and transformed back to the physical space again. The critical environmental condition is selected from contour surfaces, which are the combinations of transformed variables. Xiang and Liu [20] used the IFORM to predict the probabilistic fatigue life. A further simplification of the IFORM is the so-called environmental contour method (ECM), which ignores the variability of the response and assumes that the critical environmental condition is located on the N-year contour surface. As not many simulation realizations are required, the ECM have been widely used to estimate the extreme response induced by wave loads. Li et al. [21] investigated the extreme response of a bottom-fixed offshore wind turbine. The contour surface corresponding to a so-called important wind speed is used to collect the critical environmental condition. Karmakar et al. [22] used the ECM to predict the long-term load of a spar and a semisubmersible floating wind turbine. Canning et al. [23] perform a long-term reliability analysis of a wave energy converter with ECM.

Nevertheless, for the response of a floating wind turbine the ECM may be not applicable due to the monotonic performance of wind force and the complete IFORM without omission of the response should be used. This problem has been reported in previous studies [24-26].

In this study, a modified environmental contour method is proposed to estimate the long-term extreme response of offshore renewable energy system. The modified method considers the variability of the response by checking multiple environmental contours of different return periods. In this way, the non-monotonic behaviour of wind turbine is covered. The modified method is used to estimate the 50-year extreme response of a hybrid offshore renewable energy system. The hybrid system is based on the combination of a floating wind turbine, a WEC and two tidal turbines.

2. Model description

The hybrid concept addressed in this study, namely 'HWNC' (Hywind-Wavebob-NACA_638xx Combination, see Fig. 1), is based on the combination of the spar type floating wind turbine Hywind [27], the two-body floating WEC 'Wavebob' and two tidal turbines with tidal turbines with NACA_638xx airfoil series. The WEC, designed to move only in heave mode relative to the platform while no relative surge, sway, roll, pitch and yaw motions are allowed, is connected to the platform through mechanical facilities. Two tidal turbines are installed to harvest energy from the sea current. The main dimensions of the HWNC concept are presented in Table 1 and the inertial properties of each component are listed in Table 2.

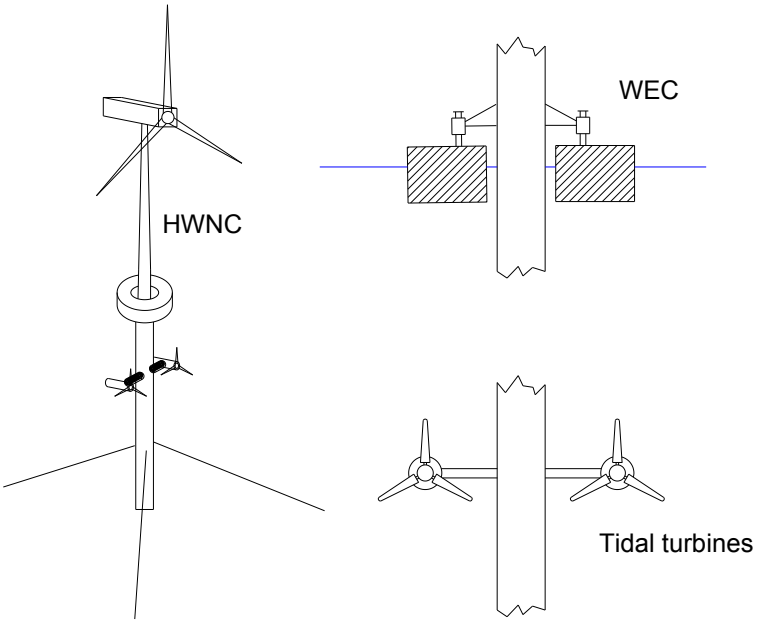

Fig. 1. HWNC concept.

Table 1
Main dimensions of the HWNC.

	Item	Value
Platform	Draft	120 m
	Tower base above still water level (SWL)	10 m
	Depth to top of taper below SWL	4 m
	Depth to bottom of taper below SWL	12 m
	Platform diameter above taper	6.5 m
	Platform diameter below taper	9.4 m
WEC	Draft	4 m
	Outer diameter	20 m
	Inner diameter	10 m
Tidal turbine	Depth below SWL	46.5 m
	Rotor diameter	10 m

Table 2
Inertial properties of subsystem.

	Item	Value
Platform	Total mass	6,995,130 kg
	Centre of mass (CM) below SWL	89.9 m
	Roll inertia about CM	4,229,230,000 kg·m^2
	Pitch inertia about CM	4,229,230,000 kg·m^2
	Yaw inertia about CM	164,230,000 kg·m^2
WEC	Total mass	1,442,000 kg
	CM below SWL	0 m
	Roll inertia about CM	3,139,900 kg·m^2
	Pitch inertia about CM	3,139,900 kg·m^2
	Yaw inertia about CM	6,022,200 kg·m^2

The HWNC is operated at sea site with a water depth of 320 m and moored by three slack catenary lines. The fairleads are connected to the platform at 70 m below the still water level. Fig. 2 displays the configuration of the mooring system. The three lines are oriented at 60°, 180°, and 300° about the vertical axis. The relevant properties of the mooring lines are listed in Table 3.

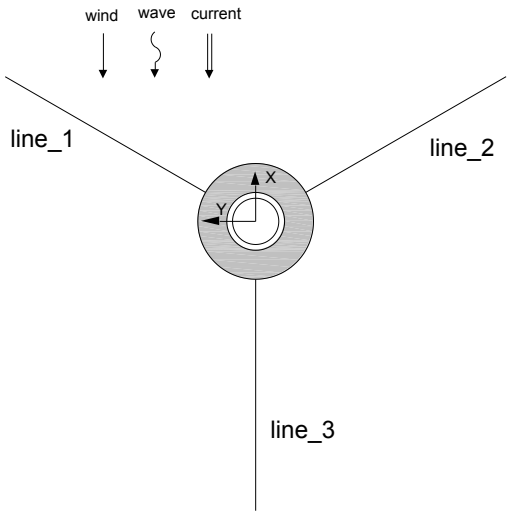

Fig. 2. Configuration of mooring lines.

Table 3
Mooring line properties.

Item	Value
Depth to anchors	320 m
Depth of fairleads	70 m
Radius to anchors	853.87 m
Radius to fairleads	5.2 m
Unstretched mooring line length	902.2 m
Mooring line diameter	0.09 m
Equivalent mooring line mass density	77.7066 kg/m
Equivalent mooring line extensional stiffness	384,243,000 N

3. Numerical model and validation

3.1. modelling

The numerical code used to perform the coupled simulation in this work is based on the combination of WindSloke developed by Li et al. [28] and WEC-Sim [29] developed under the collaboration between the National Renewable Energy Laboratory (NREL) and the Sandia National Laboratories. The aerodynamic module of WindSloke is used in this work to calculate the unsteady wind turbine thrust force by a modified blade element momentum (BEM) method. The same method is used to compute the tidal turbine thrust forces. The unsteadies of the inflow caused by platform motions is considered with a dynamic wake model [30]. WEC-Sim is a wave energy converter simulation tool with the ability to model offshore systems that are comprised of rigid bodies, PTO systems and mooring systems. WEC-Sim computes the hydrodynamic forces acting on the floating bodies based on the combination of potential flow theory and Morison equation.

Three rigid bodies are established in the numerical model of the HWNC. The spar platform and the WEC are treated as two independent floating bodies and their hydrodynamic interactions are considered. The two components are connected by the PTO facility, which is numerically treated as a spring & damper system. The stiffness coefficient K is set to 5 kN and the damping coefficient B is set to 80 kN·s/m. The wind turbine is regarded as a non-hydro body, which is rigidly mounted on the platform. Please note that deflection of the tower is not considered in this study. The mooring line is modelled with the lumped-mass approach, which divides the mooring line into a series of evenly-sized segment represented by connected nodes and spring & damper systems. The lumped-mass approach merely models the axial properties of the mooring lines while the torsional and bending properties are neglected. The effects of wave kinematics and any other external loads on the lines are also ignored in the lumped-mas model.

3.2. Validation

Since the thrust forces acting on the wind turbine and the tidal turbines are simulated with the same approach, only aerodynamic force is validated here. Firstly, the steady aerodynamic performance of the

wind turbine is simulated. Fig. 3 displays the steady aerodynamic performance of the wind turbine, in terms of thrust force and rotor power output.

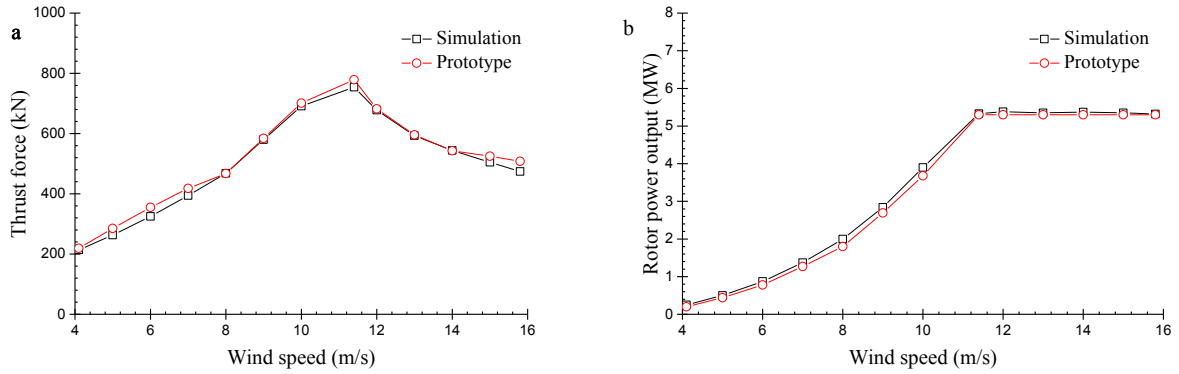

Fig. 3. Aerodynamic performance of the wind turbine. (a) thrust force; (b) rotor power output.

For a floating wind turbine, the wind force acting on the rotor is unsteady due to the aero-hydro couplings. To validate the unsteady aerodynamic performance, the wind turbine thrust force is simulated under a set of sinusoidal winds and the simulation results are compared with those obtained by FAST (version v7.02.00d-bjj) [31]. The speed of sinusoidal wind is defined by

$$V(t) = V_0 + \sin(\omega t) \tag{1}$$

where V_0 is the mean wind speed and ω is the varying frequency. The control module in FAST is switched off so that the rotor speed and the blade pitch angle are fixed in the simulations. Fig. 7 displays time series of the unsteady wind turbine thrust forces predicted by the simulation tool and FAST.

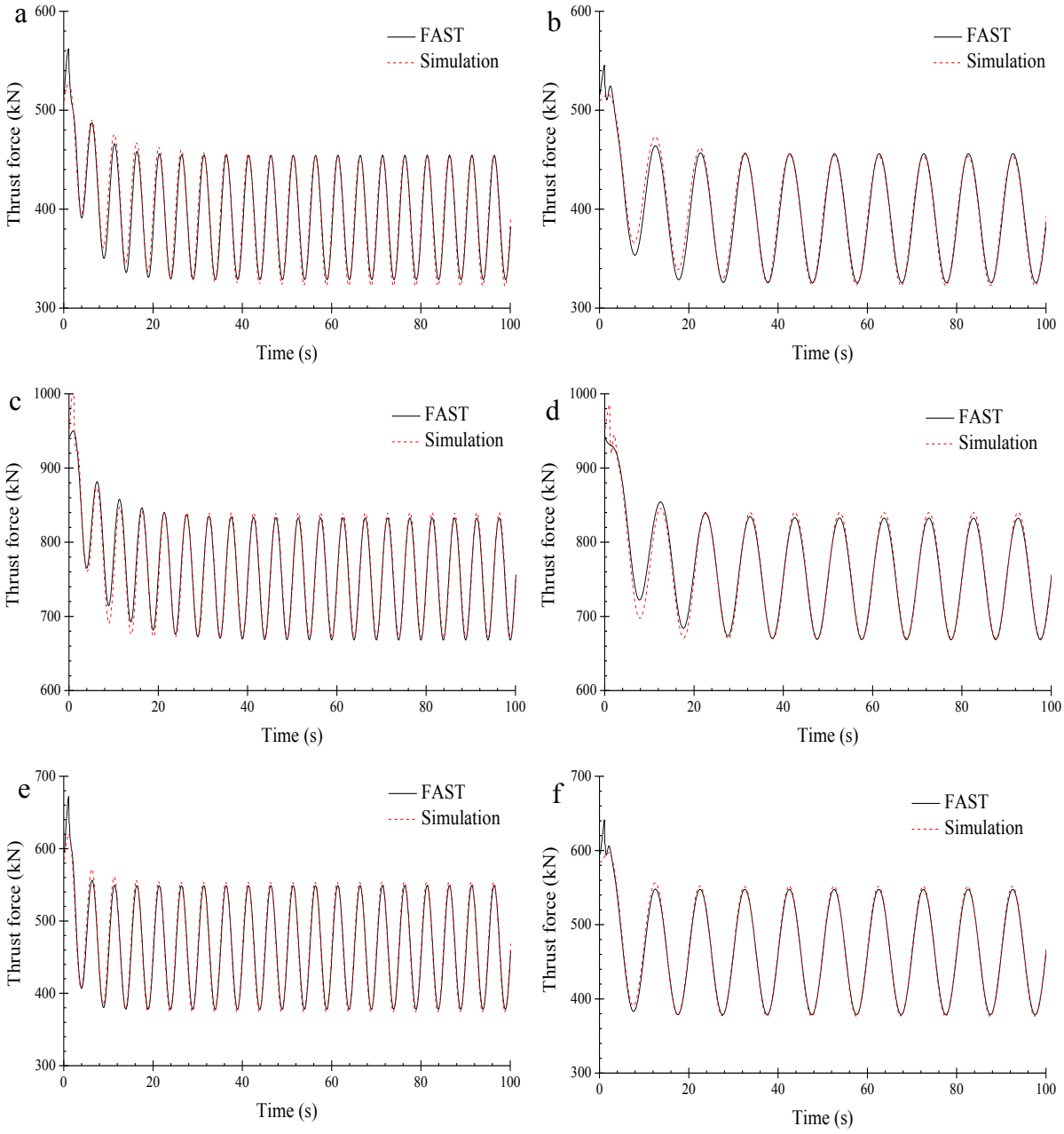

Fig. 4. Times series of unsteady wind turbine thrust forces. (a) V_0= 8 m/s, ω = 1.26 rad/s; (b) V_0 = 8 m/s, ω = 0.63rad/s; (c) V_0 = 11.4 m/s, ω = 1.26 rad/s; (d) V_0 = 11.4 m/s, ω = 0.63 rad/s; (e) V_0 = 14 m/s, ω = 1.26 rad/s; (f) V_0 = 14 m/s, ω = 0.63 rad/s.

The model test of a spar type floating wind turbine conducted by Koo et al. [32] is used to validate the numerical modelling of aero-hydro couplings. The spar type floating wind has an in identical platform geometry with the Hywind, despite that the mass and inertia of the platform were changed (see Table 4). Furthermore, the mooring system was also somewhat varied (see Table 5). Please refer to [32] for more details of the model test set-up. The numerical model of the floating wind turbine used by Koo et al. [32] is developed and the simulation results are compared with the model test measurement to validate the aero-hydro couplings. White noise waves were generated in the model test to get the response amplitude operator (RAO) of platform motions in the presence of rated wind turbine thrust

force. The same procedure is employed in the numerical simulation. Fig. 5 compares the RAOs acquired by the simulation tool and the experiment.

Table 4
Mass property of the platform in [32].

Item	Value
Mass	7,980,000 kg
Roll gyration	53.54 m
Pitch gyration	53.54 m
Yaw gyration	3.68 m

Table 5
Mooring system in [32]

Item	Value
Anchor radius	445 m
Anchor depth	200 m
Fairlead radius	5.2 m
Fairlead depth	70 m

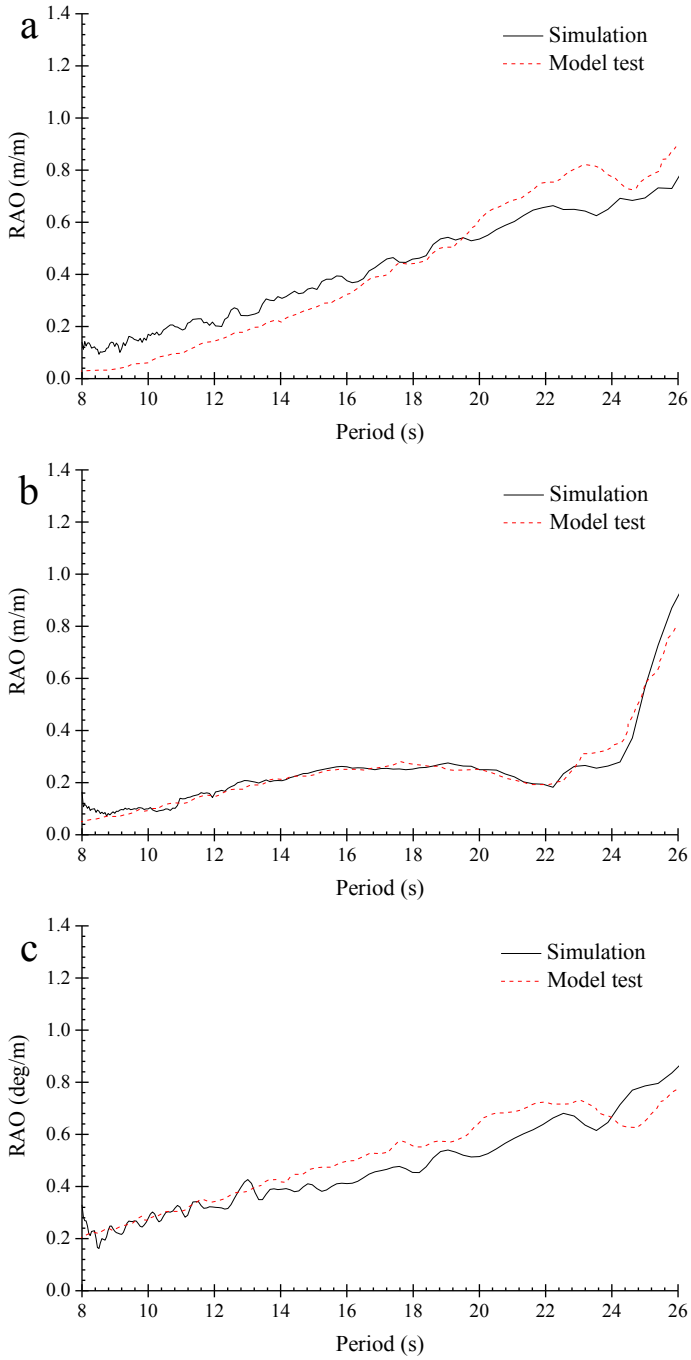

Fig. 5. RAOs of platform motions. (a) surge motion; (b) heave motion; (c) pitch motion.

4. Long-term extreme analysis

4.1. Full long-term analysis

The full long-term analysis method is a very straightforward approach to predict the extreme response, which considers all the combinations of environmental condition parameters (see Fig. 6). The FLTA method calculates the long-term cumulative distribution function (CDF) just by integrating the short-term probability functions and the corresponding environmental condition parameters

171 $$F_X^{LT}(x) = \int F_{X|S}^{ST}(x|s) f_S(s) ds \quad (2)$$

172 where x is response variable and s is the environmental condition parameter. F_X^{LT} is the long-term CDF
173 of response while $F_{X|S}^{ST}$ is the short-term CDF at a given environmental condition s. f_S is the probability
174 density function used to describe the environmental condition. In this study, we use the 1-hr short-term
175 CDF to extrapolate the 50-year long-term extreme response. Since wind speed u, wave height h and
176 wave period t is the dominating environmental parameters, Eq. (2) can be re-written as

177 $$\begin{aligned} F_{X_{50-year}}^{LT}(x) &= \left[F_{X_{1-hr}}^{LT}(x) \right]^{50\times 365.25\times 24} \\ F_{X_{1-hr}}^{LT}(x) &= \iiint F_{X_{1-hr}|U,H,T}^{ST}(x|u,h,t) f_{U,H,T}(u,h,t) du dh dt \end{aligned} \quad (3)$$

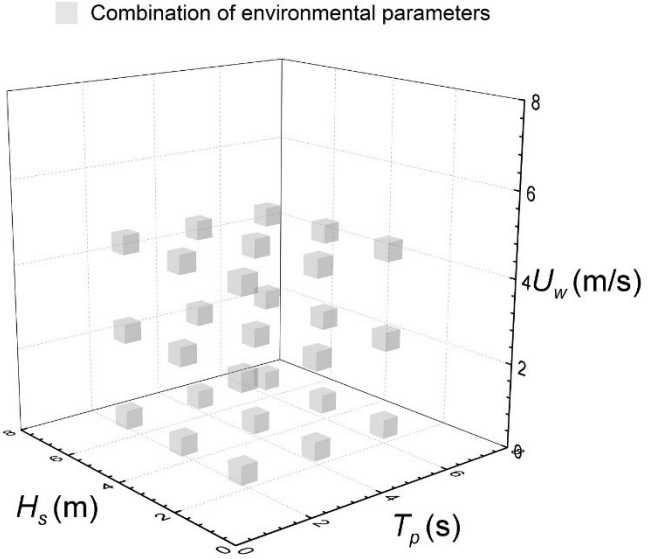

178
179 Fig. 6. Combinations of environmental parameters.

180 ## *4.2. Modified environmental contour method*

181 As shown in Eq. (3), the FLTA method requires massive simulations and it can be extremely time
182 consuming. Therefore, simplified methods have been developed to enhance the efficiency. The
183 environmental contour method is one of these methods, which is based on the IFORM and assumes that
184 the long-term extreme values are just affected by several critical environmental conditions. The ECM
185 aims at selecting the most important environmental condition, namely the essential combination of
186 environmental parameters, located on the contour surface with a desired N-year return period.

187 $$F_{X_{1-hr,N-year}}^{LT} \approx F_{X_{1-hr}|U_w,H_s,T_p}^{ST}(x|u_N,h_N,t_N) \quad (4)$$

188 (u_N, h_N, t_N) is the environmental parameter leading to the largest extreme response in the N-year return
189 period contour surface. The generation of the environmental contour surface is based on the Rosenblatt
190 transformation, which transforms the environmental parameter X from the initial X-space into a
191 nonphysical U-space (see Fig. 7).

192 $$U = T_2(T_1(X)) \quad (5)$$

$$T_1 : Y = \begin{pmatrix} F_1(x_1) \\ \cdots \\ F_{k|1,\ldots,k-1}(x_k \,|x_1,\ldots,x_{k-1}) \\ F_{n|1,\ldots,n-1}(x_n \,|x_1,\ldots,x_{n-1}) \end{pmatrix} \tag{6}$$

$$T_2 : U = \begin{pmatrix} \Phi^{-1}(y_1) \\ \cdots \\ \Phi^{-1}(y_k) \\ \Phi^{-1}(y_n) \end{pmatrix} \tag{7}$$

Φ is CDF of the standard normal distribution. In the U-space, all combinations of transformed environmental parameters with respect to N-year return period are located on a sphere with radius r

$$r = \Phi^{-1}\left(1 - \frac{1}{N \times 365.25 \times 24}\right) \tag{8}$$

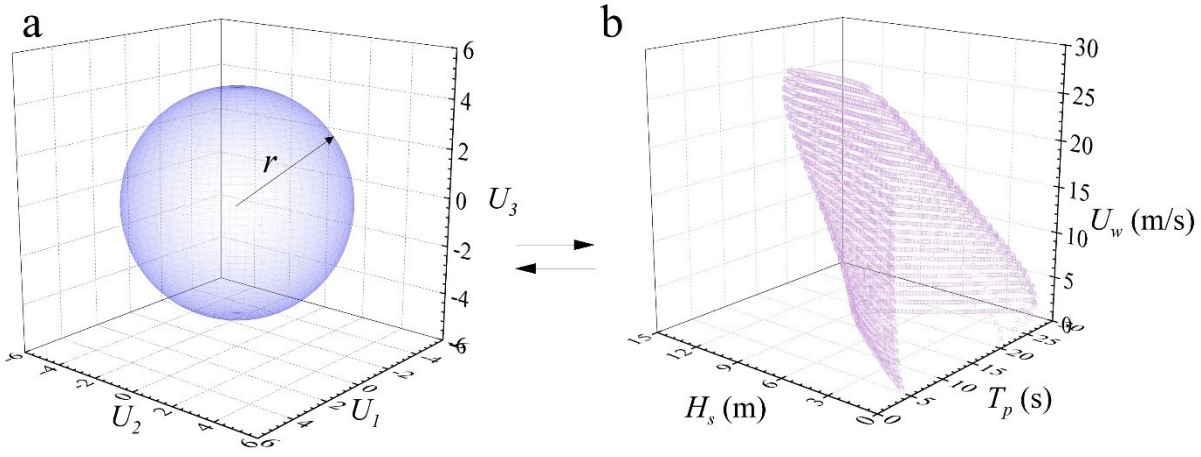

Fig. 7. Rosenblatt transformation. (a) U-space; (b) X-space.

Then the environmental contour surface can be obtained by transforming the sphere back to the U-space. The procedures of ECM are outlined in Fig. 8.

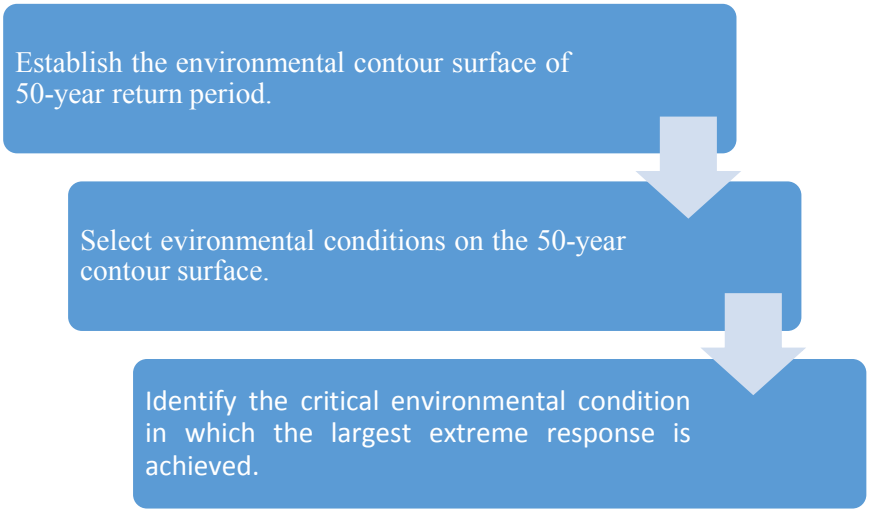

Fig. 8. Procedures of ECM.

The above discussions outline the basic procedures of ECM, which is actually a simplification of IFORM, ignoring the variability of response and decoupling the response variability and the environment. It inherently implies that the ECM assumes the actual critical environmental condition to be close to the counter surface in X-space or the sphere in U-space with respect to the 50-year return period. Due to this assumption, which is also the limitation of ECM, ECM is not applicable to a floating wind turbine [24, 25]. This is because the wind force is not monotonic with the wind speed, especially around the cut-out wind speed. As shown in Fig. 9, the thrust force reaches the maximum value at rated wind speed (11.4 m/s) and drops gradually as the wind speed continues increasing. If the wind speed exceeds the cut-out speed 25 m/s, the wind turbine is parked and no wind force is applied on the rotor. In this case, the responses induced by wind force are higher in operational state and lower in parked state. Moreover, a discontinuity appears at 25 m/s. Consequently, the omission of response variability is not reasonable. In this circumstance, the IFORM should be used. Although the IFORM is already a simplification than the FLTA, it is still more complex than the ECM and requires massive simulations. Therefore, a modification is made to the ECM in this study, which considers the variability of response by checking multiple environmental contour surfaces.

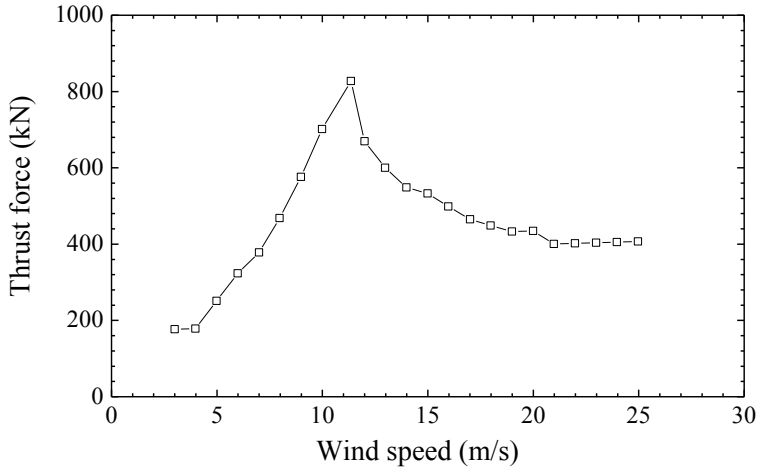

Fig. 9. Relationship between thrust force and wind speed at hub height.

Basically, the procedures of the modified ECM is similar with those of the EMC, which can be regarded as an expansion of the ECM while still a simplification of the IFORM. The main idea of the modified ECM is to include multiple important contour surfaces rather than the 50-year one alone. As shown in Fig. 10, the first step is to select a set of wind speeds with respect to different return periods and the corresponding most probable wave heights and wave periods based on a joint wind-wave distribution model. Simulations are afterwards performed to acquire the extreme values with respect to these selected environmental parameters. The first step is introduced to find the wind speed in which the non-monotonic behaviour of the wind turbine is the most significant. Subsequently, the *N*-year return period corresponding to a response peak as well as the 50-year return period are selected. A response peak is observed because the non-monotonic behaviour of the wind turbine is remarkable at this wind speed. It should be noted that the wind speed at 10 m above the mean sea level is used to

represent the environmental conditions in this study, therefore the cut-out speed measured in Fig. 10 is not 25 m/s (the cut-out wind speed 25 m/s refers to hub height). The hub height wind speed is not used because the joint wind-wave wave probability distribution model used in this study is only applicable to wind speed at 10 m height. Finally, search for the critical environmental condition on the selected multiple contour surfaces (including the 50-year one). In this way, the variability of response is considered by checking multiple contour surfaces with different return periods. If all the contour surfaces within 50-year return period is included, then the modified ECM will become the IFORM. If only the 50-year contour surface is identified (no response peak occurs), the modified ECM becomes the ECM.

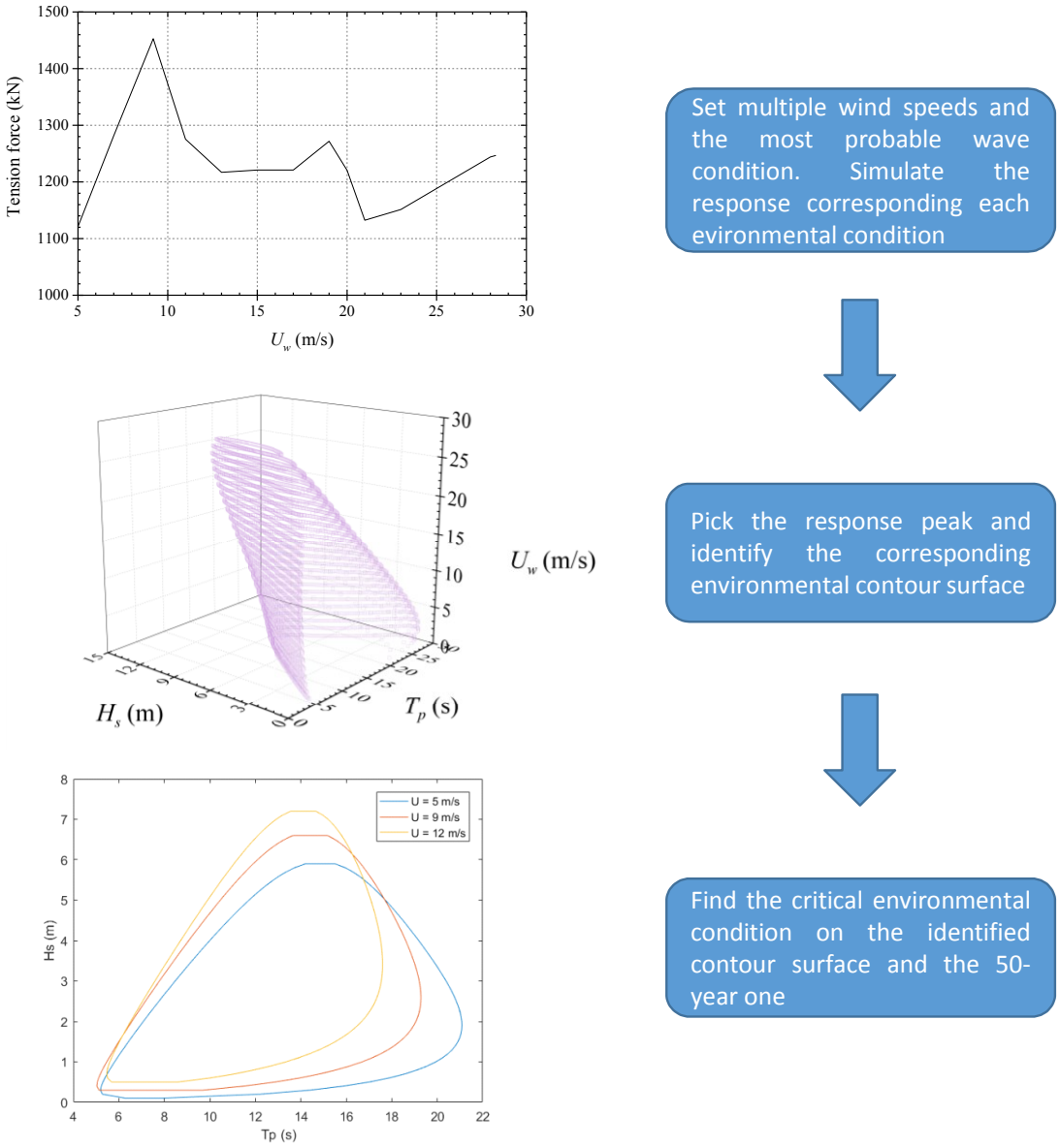

Fig. 10. The procedure of modified ECM.

For an *N*-year return period identified by the modified ECM, assuming each 1-hr period is independent, the 1-hr extreme CDF of *N*-year return period can be used to extrapolate the 1-hr extreme CDF of 50-year return period

$$F^{LT}_{X_{1-hr,50-year}}(x)=\left[F^{LT}_{X_{1-hr,N-year}}(x)\right]^{50/N}\approx\left[F^{ST}_{X_{1-hr}|U_w,H_s,T_p}(x|u_N,h_N,t_N)\right]^{50/N} \tag{9}$$

As illustrated by Eq. (9), the modified ECM uses the 1-hr short-term CDF to approximate the 1-hr long-term CDF of *N*-year and then extrapolate it to acquire the 1-hr long-term CDF of 50-year return. Comparatively, the standard ECM merely use the 1-hr short-term CDF to get the 50-year extreme values. The two methods are identical if only the 50-year contour surface is identified.

Given that the critical environmental condition has been identified by the modified ECM, a certain amount of simulations is required to extrapolate the $F^{LT}_{1-hr,N-year}$. Assuming that the extreme response of an offshore structure converges to the Gumbel distribution

$$F(x)=\exp(-\exp(-(x-\mu)/\sigma)) \tag{10}$$

Then the most probable 50-year extreme value is given by Eq. (11). In the following part of this paper, the extreme response refers to the most probable 50-year extreme response unless a special announcement is made.

$$M_{X_{1-hr,50-year}}=\mu+\sigma\cdot\ln(50/N) \tag{11}$$

One way to examine whether sufficient simulation realizations are performed is to check the 95% confidence interval. Assuming that the errors of the extreme values are normal distributed, the confidence interval is given by

$$\begin{aligned}&M_{CI\pm}(n)=\hat{M}(n)+t_{2.5\%,n}\sqrt{\mathrm{var}(\hat{M}(n))/n}\\&\hat{M}(n)=\hat{\mu}(n)+\hat{\sigma}\ln(50/N)\end{aligned} \tag{12}$$

where $\hat{\mu}$ and $\hat{\sigma}$ are the estimated parameters of the Gumbel distribution based on n simulation realizations. $t_{2.5\%,n}$ is the 97.5% factile value Student's *t*-distribution with n degrees of freedom. A parameter *CI* is introduced to value whether the number of realizations is sufficient

$$CI(n)=\frac{\hat{M}_{CI+}(n)-\hat{M}_{CI-}(n)}{\hat{M}(n)} \tag{13}$$

It is found that estimating μ and σ by Eq. (10) directly requires a huge amount of simulation realizations to acquire satisfactory approximation. Therefore, Eq. (10) is transformed to a linear equation and rewritten by Eq. (14). Fig. 11 displays the estimation of parameters μ and σ for mooring line tension force.

$$x=\sigma\left\{-\ln\left[-\ln\left(F\right)\right]\right\}+\mu \tag{14}$$

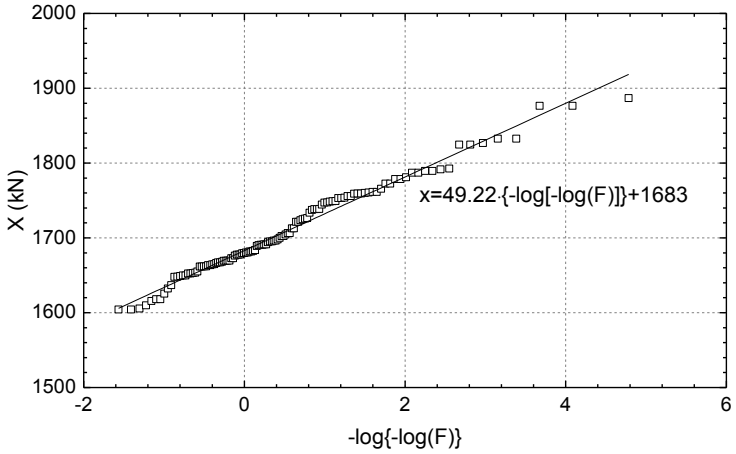

Fig. 11. Estimation of parameters μ and σ for mooring line tension force.

Different numbers of simulation realizations are checked and the results are listed in Table 6. As shown, 120 simulation realizations are sufficient to produce reliable prediction. Therefore, the following extreme responses presented in this study are based on 120 simulation realizations.

Table 6
CI with different number of simluations realizations.

n	Shear force (kN)	Bending moment (kN·m)	Tension force (kN)
80	1.6%	2.5%	1.4%
120	1.3%	2.1%	1.1%

4.3. Joint wind wave probability distribution model

The joint wind-wave distribution model developed by Li et al. [21] is used in this study. The model is based on the filed measurement in the North Sea centre from 2001 to 2010, which consists of a marginal distribution of wind speed at 10 m above the mean sea level U_w, a conditional distribution of wave height H_s given U_w, and a conditional distribution of wave period T_p given U_w and H_s,

$$f_{U_w,H_s,T_t}(u,h,t) = f_{U_w}(u)\cdot f_{H_s|U_w}(h|u)\cdot f_{T_p|U_w,H_s}(t|u,h) \tag{15}$$

The wind speed follows the Weibull distribution

$$f_{U_w}(u) = \frac{\alpha_U}{\beta_U}\left(\frac{u}{\beta_U}\right)^{\alpha_U-1}\cdot\exp\left[-\left(\frac{u}{\beta_U}\right)^{\alpha_U}\right] \tag{16}$$

The conditional wave height also converges to the Weibull distribution

$$f_{H_s|U_w}(h|u) = \frac{\alpha_H}{\beta_H}\left(\frac{u}{\beta_H}\right)^{\alpha_H-1}\cdot\exp\left[-\left(\frac{u}{\beta_H}\right)^{\alpha_H}\right]$$

$$\alpha_H = a_1 + a_2\cdot u^{a_3} \tag{17}$$

$$\beta_H = b_1 + b_2\cdot u^{b_3}$$

Given a combination of U and H, the wave period converges to the log-normal distribution

$$f_{T_p|U_w,H_s}(t|u,h)=\frac{1}{\sqrt{2\pi}\sigma_{\ln(T)}t}\cdot\exp\left[-\frac{1}{2}\left(\frac{\ln(t)-\mu_{\ln(T)}}{\sigma_{\ln(T)}}\right)^2\right]$$

$$\mu_{\ln(T)}=\ln\left(\frac{\mu_T}{\sqrt{1+v_T^2}}\right),\sigma_{\ln(T)}=\sqrt{\ln(v_T^2+1)} \tag{18}$$

$$\mu_T=\bar{t}(h)\cdot\left[1+\theta\left(\frac{u-\bar{u}(h)}{\bar{u}(h)}\right)^{\gamma}\right],v_T=k_1+k_2\cdot\exp(hk_3)$$

$$\bar{t}(h)=e_1+e_2\cdot h^{e_3},\bar{u}(h)=f_1+f_2\cdot h^{f_3}$$

The parameters that used to specify the joint distribution model can be found in [21].

In a realistic sea site, the wind speed varies with the height so that the blades will experience different wind speeds due to the rotor rotation (see Fig. 12). To calculate the wind force realistically, a power law profile with exponent α equal to 0.1 is used to describe the wind speeds at different heights.

$$U_Z(z)=U_w\cdot\left(\frac{z}{10}\right)^{\alpha} \tag{19}$$

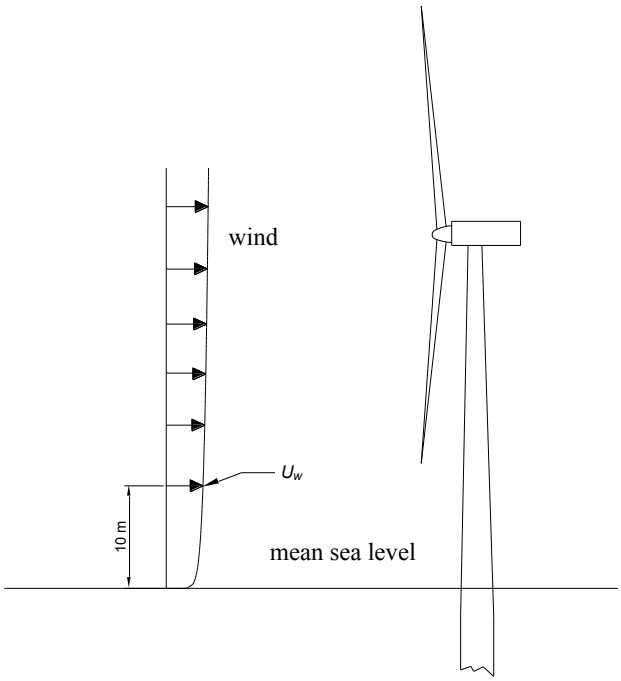

Fig. 12. Wind profile.

5. Simulation and results

This section will examine the extreme response of the HWNC with the modified environmental contour method proposed in this study.

The fore-aft tower base bending moment is firstly measured. Fig. 13 shows the first step of the modified ECM. Generally, the behaviour of the bending moment is monotonic despite that a tiny response peak is observed at U_w = 9.2 m/s (corresponding to 11.4 m/s at hub height). It can be simply explained by that the response is governed by both wind force and wave load and thereby a response

peak appears when the wind turbine thrust force reaches maximum value at rated wind speed. According to the variation trend, wave load plays a more important role than the wind force. Based on the first step of the modified ECM, two contour surfaces are selected. The identified critical environmental condition and the extreme response are listed in Table 7. Since the critical condition selected by the two methods is located on the 50-year contour surface, it is obvious that the two methods predict identical extreme response. As discussed in Section 4.2, the ECM is valid when the wave loads play the dominating role, on which condition the critical environmental condition is close to the 50-year contour surface. Therefore, inclusion of environmental conditions from other contour surfaces will not increase the accuracy.

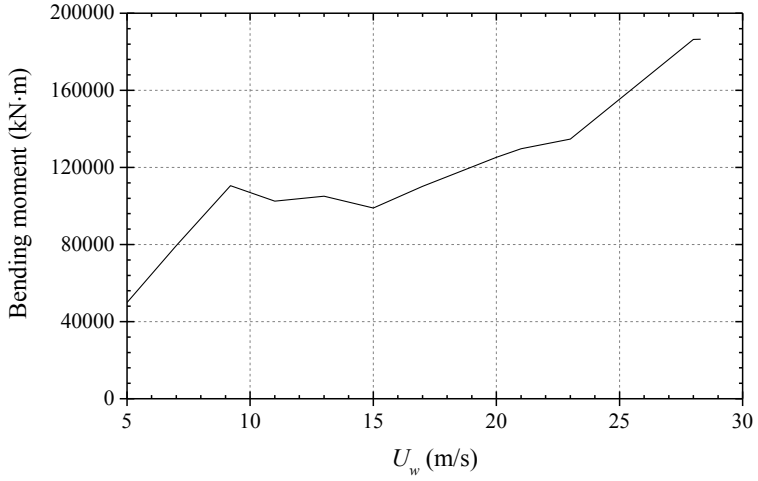

Fig. 13. Selection of contour surface.

Table 7
Selected critical environmental conditions and extreme bending moment

Method	Selected environmental parameters			Return period (year)	Extreme (kN·m)
	U_w (m/s)	H_s (m)	T_p (s)		
modified ECM	24.5	11.98	13.6	50	2.53×10^5
ECM	24.5	11.98	13.6	50	2.53×10^5

Mooring line 2 is selected as another representation of the structural response. The 1-hr extreme tension force with a return period of 50 years is investigated. As shown in Fig. 14, two response peaks are observed around U_w = 9.2 m/s and U_w = 19 m/s. Therefore, three contour surfaces are included in the modified ECM. Apparently, the wind force dominates the response and the non-monotonic behaviour of the response is quite notable, implying that the assumption of ECM is violated.

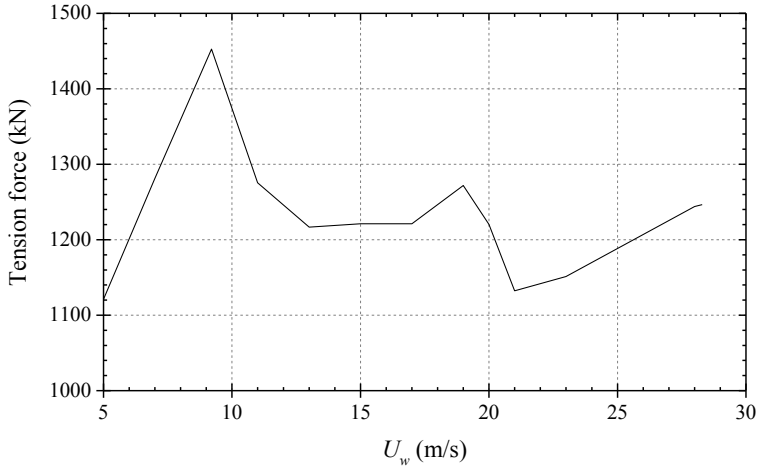

Fig. 14. Selection of contour surface.

Based on the first step of modified ECM, three contour surfaces are identified whereas the ECM still seeks the critical environmental condition from the 50-year one. Fig. 15 shows the critical environmental conditions selected by the two methods. Since the mooring line tension is dominated by the wind force, these two methods both identify U_w = 9.2 m/s as the critical wind speed. Nevertheless, the combination of significant wave height and spectrum period picked by these two methods are quite different. The modified ECM selects H_s = 6.3 m, T_p=14.2 s as the critical environmental condition whereas the critical parameters identified by the ECM is H_s = 8.75 m, T_p =15.0 s. This is because the two select environmental conditions from different contours. Apparently, the ECM selects a rarer wave condition.

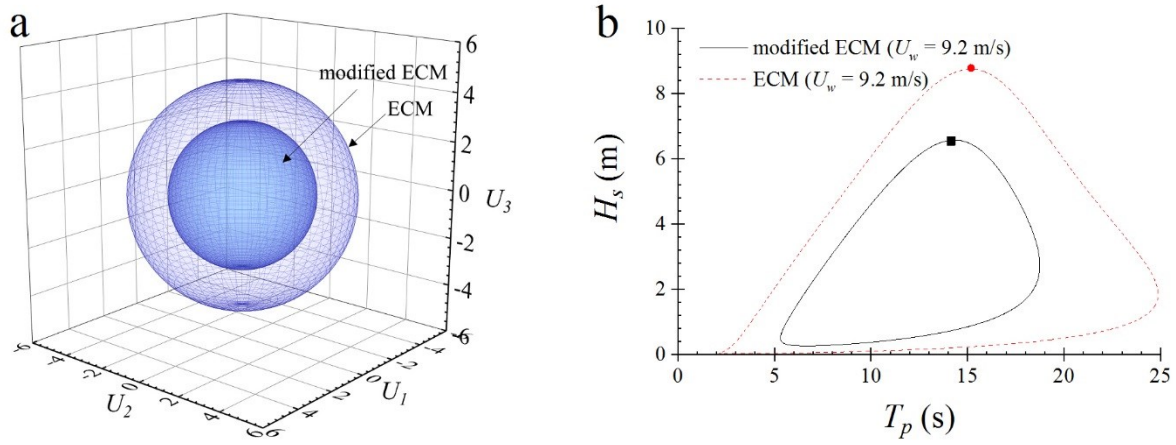

Fig. 15. The selected critical environmental condition. (a) U-space; (b) X-space.

Table 8 lists the extreme mooring line tension obtained with the two methods. The critical environmental condition identified by the ECM is far from the real one and the ECM underestimates the extreme response by 10% approximately. It reflects the advantage of the modified ECM against the ECM. For response that purely dominated by wave forces, the short-term extreme response with respect to 0.04-year return period is lower than the 50-year extreme value. Extrapolating the 0.04-year return period extreme to the 50-year value by Eq. (9), the modified ECM may produce similar results with the

ECM. But it is not the case for the mooring line tension which is dominated by the wind forces rather than the wave forces. In fact, a rare wave condition won't increase the extreme tension force much. When the 0.04-year short-term extreme is extrapolated, the modified ECM will produce a much larger extreme response.

Table 8
Selected critical environmental conditions and extreme mooring line tension

method	Selected environmental parameters			Return period (year)	Extreme (kN)
	U_w (m/s)	H_s (m)	T_p (s)		
modified ECM	9.2	6.3	14.2	0.04	2134
ECM	9.2	8.75	15.0	50	1942

6. Conclusions

This study deals with long-term extreme response of an integrated offshore renewable energy system combining a floating wind turbine, a wave energy converter and two tidal turbines. For offshore floating structures subject to wave excitations, the ECM has been validated to produce accurate results. Nevertheless, it is not applicable to the integrated device in this study due to the non-monotonic behaviour of the wind turbine. A modified environmental contour method is thus proposed to address this problem, which is an expansion of the ECM and still a simplification of the inverse first-order reliability method. Unlike the ECM which seeks the critical environmental condition on the 50-year contour surface, the modified ECM considers the non-monotonic behaviour of wind turbine by checking multiple contour surfaces. The extra contour surfaces are selected based on important wind speeds, at which the non-monotonic performance of the wind turbine is most remarkable. For the extreme mooring line tension force, the critical environmental selected by the modified ECM is located on the 0.04-year contour surface rather than the 50-year one and the modified ECM suggests an extreme value 10% larger than that given by the ECM. It implies that the critical environmental condition identified by the modified ECM is closer to the real one.

Acknowledgement

The authors would like to acknowledge China Scholarship Council for the financial support (No. 201506230127).

References

[1] L. Li, Z. Yuan, Y. Gao, X. Zhang, Wave force prediction effect on the energy absorption of a wave energy converter with real-time control, IEEE T Sustain Energ (2018) 1-1.

[2] L. Li, Y. Gao, Z.Q. Hu, Z.M. Yuan, S. Day, H.R. Li, Model test research of a semisubmersible floating wind turbine with an improved deficient thrust force correction approach, Renew Energ 119 (2018) 95-105.

[3] B. Whitby, C.E. Ugalde-Loo, Performance of Pitch and Stall Regulated Tidal Stream Turbines, IEEE T Sustain Energ 5(1) (2014) 64-72.
[4] L. Li, Z. Hu, J. Wang, Q. Hu, Dynamic Responses of a Semi-type Offshore Floating Wind Turbine, 33rd International Conference on Ocean, Offshore and Arctic Engineering, American Society of Mechanical Engineers, 2014.
[5] L. Li, Y. Liu, Z. Yuan, Y. Gao, Wind field effect on the power generation and aerodynamic performance of offshore floating wind turbines, Energy 157 (2018) 379-390.
[6] M.H. Nehrir, C. Wang, K. Strunz, H. Aki, R. Ramakumar, J. Bing, Z. Miao, Z. Salameh, A Review of Hybrid Renewable/Alternative Energy Systems for Electric Power Generation: Configurations, Control, and Applications, IEEE T Sustain Energ 2(4) (2011) 392-403.
[7] A. Aubault, M. Alves, A. Sarmento, D. Roddier, A. Peiffer, Modeling of an oscillating water column on the floating foundation WindFloat, International Conference on Ocean, Offshore and Arctic Engineering, American Society of Mechanical Engineers, 2011, pp. 235-246.
[8] M.J. Muliawan, M. Karimirad, T. Moan, Dynamic response and power performance of a combined spar-type floating wind turbine and coaxial floating wave energy converter, Renew Energ 50 (2013) 47-57.
[9] L. Wan, Z. Gao, T. Moan, Experimental and numerical study of hydrodynamic responses of a combined wind and wave energy converter concept in survival modes, Coast Eng 104 (2015) 151-169.
[10] L. Wan, M. Greco, C. Lugni, Z. Gao, T. Moan, A combined wind and wave energy-converter concept in survival mode: Numerical and experimental study in regular waves with a focus on water entry and exit, Appl Ocean Res 63 (2017) 200-216.
[11] L. Wan, Z. Gao, T. Moan, C. Lugni, Experimental and numerical comparisons of hydrodynamic responses for a combined wind and wave energy converter concept under operational conditions, Renew Energ 93 (2016) 87-100.
[12] C. Michailides, C. Luan, Z. Gao, T. Moan, Effect of flap type wave energy converters on the response of a semi-submersible wind turbine in operational conditions, International Conference on Ocean, Offshore and Arctic Engineering, American Society of Mechanical Engineers, 2014, pp. V09BT09A014-V09BT09A014.
[13] L. Li, Y. Gao, Z.M. Yuan, S. Day, Z.Q. Hu, Dynamic response and power production of a floating integrated wind, wave and tidal energy system, Renew Energ 116 (2018) 412-422.
[14] L. Li, Z. Cheng, Z. Yuan, Y. Gao, Short-term extreme response and fatigue damage of an integrated offshore renewable energy system, Renew Energ 126 (2018) 617-629.
[15] E.E. Bachynski, T. Moan, Point absorber design for a combined wind and wave energy converter on a tension-leg support structure, International Conference on Ocean, Offshore and Arctic Engineering, American Society of Mechanical Engineers, 2013, pp. V008T09A025-V008T09A025.
[16] R.G. Coe, C. Michelen, A. Eckert-Gallup, C. Sallaberry, Full long-term design response analysis of a wave energy converter, Renew Energ (2017).

413 [17] P. Agarwal, L. Manuel, Simulation of offshore wind turbine response for long-term extreme load
414 prediction, Eng Struct 31(10) (2009) 2236-2246.
415 [18] P. Videiro, T. Moan, Efficient evaluation of long-term distributions, International Conference on
416 Offshore Mechanics and Arctic Engineering (OMAE), 1999.
417 [19] S.R. Winterstein, T.C. Ude, C.A. Cornell, P. Bjerager, S. Haver, Environmental parameters for
418 extreme response: Inverse FORM with omission factors, Proceedings of the ICOSSAR-93, Innsbruck,
419 Austria (1993) 551-557.
420 [20] Y. Xiang, Y. Liu, Application of inverse first-order reliability method for probabilistic fatigue life
421 prediction, Probabilistic Engineering Mechanics 26(2) (2011) 148-156.
422 [21] L. Li, Z. Gao, T. Moan, Joint distribution of environmental condition at five european offshore
423 sites for design of combined wind and wave energy devices, Journal of Offshore Mechanics and Arctic
424 Engineering 137(3) (2015) 031901.
425 [22] D. Karmakar, H. Bagbanci, C.G. Soares, Long-Term Extreme Load Prediction of Spar and
426 Semisubmersible Floating Wind Turbines Using the Environmental Contour Method, Journal of
427 Offshore Mechanics and Arctic Engineering 138(2) (2016) 021601.
428 [23] J. Canning, P. Nguyen, L. Manuel, R.G. Coe, On the Long-Term Reliability Analysis of a Point
429 Absorber Wave Energy Converter, International Conference on Ocean, Offshore and Arctic
430 Engineering, American Society of Mechanical Engineers, 2017, pp. V010T09A024-V010T09A024.
431 [24] K. Saranyasoontorn, L. Manuel, On assessing the accuracy of offshore wind turbine reliability-
432 based design loads from the environmental contour method, International Journal of Offshore and Polar
433 Engineering 15(02) (2005).
434 [25] K. Saranyasoontorn, L. Manuel, Efficient models for wind turbine extreme loads using inverse
435 reliability, J Wind Eng Ind Aerod 92(10) (2004) 789-804.
436 [26] N. Aggarwal, R. Manikandan, N. Saha, Nonlinear short term extreme response of spar type floating
437 offshore wind turbines, Ocean Eng 130 (2017) 199-209.
438 [27] J.M. Jonkman, Definition of the Floating System for Phase IV of OC3, Citeseer 2010.
439 [28] L. Li, Z.Q. Hu, J. Wang, Y. Ma, Development and Validation of an Aero-hydro Simulation Code
440 for Offshore Floating Wind Turbine, J Ocean Wind Energy 2(1) (2015) 1-11.
441 [29] NWTC Information Portal. (WEC-Sim), 2017. https://nwtc.nrel.gov/WEC-Sim. (Accessed 15-
442 September 2017).
443 [30] A.R. Bramwell, D. Balmford, G. Done, Bramwell's helicopter dynamics, Butterworth-
444 Heinemann2001.
445 [31] J.M. Jonkman, M.L. Buhl Jr, FAST User's Guide, National Renewable Energy Laboratory (NREL),
446 2005.
447 [32] B.J. Koo, A.J. Goupee, R.W. Kimball, K.F. Lambrakos, Model Tests for a Floating Wind Turbine
448 on Three Different Floaters, J Offshore Mech Arct 136(2) (2014) 020907.
449